

## LETTERS

## Quantum simulation of the Dirac equation

R. Gerritsma<sup>1,2</sup>, G. Kirchmair<sup>1,2</sup>, F. Zähringer<sup>1,2</sup>, E. Solano<sup>3,4</sup>, R. Blatt<sup>1,2</sup> & C. F. Roos<sup>1,2</sup>

The Dirac equation<sup>1</sup> successfully merges quantum mechanics with special relativity. It provides a natural description of the electron spin, predicts the existence of antimatter<sup>2</sup> and is able to reproduce accurately the spectrum of the hydrogen atom. The realm of the Dirac equation—relativistic quantum mechanics—is considered to be the natural transition to quantum field theory. However, the Dirac equation also predicts some peculiar effects, such as Klein's paradox<sup>3</sup> and 'Zitterbewegung', an unexpected quivering motion of a free relativistic quantum particle<sup>4</sup>. These and other predicted phenomena are key fundamental examples for understanding relativistic quantum effects, but are difficult to observe in real particles. In recent years, there has been increased interest in simulations of relativistic quantum effects using different physical set-ups<sup>5–11</sup>, in which parameter tunability allows access to different physical regimes. Here we perform a proof-of-principle quantum simulation of the one-dimensional Dirac equation using a single trapped ion<sup>7</sup> set to behave as a free relativistic quantum particle. We measure the particle position as a function of time and study Zitterbewegung for different initial superpositions of positive- and negative-energy spinor states, as well as the crossover from relativistic to non-relativistic dynamics. The high level of control of trapped-ion experimental parameters makes it possible to simulate textbook examples of relativistic quantum physics.

The Dirac equation for a spin-1/2 particle with rest mass  $m$  is given by<sup>1</sup>

$$i\hbar \frac{\partial \psi}{\partial t} = (c\boldsymbol{\alpha} \cdot \hat{\mathbf{p}} + \beta mc^2)\psi$$

Here  $c$  is the speed of light,  $\hat{\mathbf{p}}$  is the momentum operator,  $\alpha_j$  ( $j = 1, 2, 3$ ;  $\boldsymbol{\alpha}_j = \alpha_j$ ) and  $\beta$  are the Dirac matrices (which are usually given in terms of the Pauli matrices,  $\sigma_x$ ,  $\sigma_y$  and  $\sigma_z$ ), the wavefunctions  $\psi$  are four-component spinors and  $\hbar$  is Planck's constant divided by  $2\pi$ . A general Dirac spinor can be decomposed into parts with positive and negative energies  $E = \pm \sqrt{p^2 c^2 + m^2 c^4}$ . Zitterbewegung is understood to be an interference effect between the positive- and negative-energy parts of the spinor and does not appear for spinors that consist entirely of positive-energy (or negative-energy) parts. Furthermore, it is only present when these parts have significant overlap in position and momentum space and is therefore not a sustained effect under most circumstances<sup>1</sup>. For a free electron, the Dirac equation predicts the Zitterbewegung to have an amplitude of the order of the Compton wavelength,  $R_{ZB} \approx 10^{-12}$  m, and a frequency of  $\omega_{ZB} \approx 10^{21}$  Hz, and the effect has so far been experimentally inaccessible. The existence of Zitterbewegung, in relativistic quantum mechanics and in quantum field theory, has been a recurrent subject of discussion in the past years<sup>12,13</sup>.

Quantum simulation aims to simulate a quantum system using a controllable laboratory system that underlies the same mathematical model. In this way, it is possible to simulate quantum systems that can be neither efficiently simulated on a classical computer<sup>14</sup> nor

easily accessed experimentally, while allowing parameter tunability over a wide range. The difficulties in observing real quantum relativistic effects have generated significant interest in the quantum simulation of their dynamics. Examples include black holes in Bose–Einstein condensates<sup>5</sup> and Zitterbewegung for massive fermions in solid-state physics<sup>6</sup>, neither of which have been experimentally realized so far. Also, graphene is studied widely in connection to the Dirac equation<sup>15–17</sup>.

Trapped ions are particularly interesting for the purpose of quantum simulation<sup>18–20</sup>, as they allow exceptional control of experimental parameters, and initialization and read-out can be achieved with high fidelity. Recently, for example, a proof-of-principle simulation of a quantum magnet was performed<sup>21</sup> using trapped ions. The full, three-dimensional, Dirac equation Hamiltonian can be simulated using lasers coupling to the three vibrational eigenmodes and the internal states of a single trapped ion<sup>7</sup>. The set-up can be significantly simplified when simulating the Dirac equation in 1 + 1 dimensions, yet the most unexpected features of the Dirac equation, such as Zitterbewegung and the Klein paradox, remain. In the Dirac equation in 1 + 1 dimensions, that is

$$i\hbar \frac{\partial \psi}{\partial t} = H_D \psi = (c\hat{p}\sigma_x + mc^2\sigma_z)\psi$$

there is only one motional degree of freedom and the spinor is encoded in two internal levels, related to positive- and negative-energy states<sup>7</sup>. We find that the velocity of the free Dirac particle is  $d\hat{\mathbf{x}}/dt = [\hat{\mathbf{x}}, H_D]/i\hbar = c\sigma_x$  in the Heisenberg picture. For a massless particle,  $[\sigma_x, H_D] = 0$  and, hence,  $\sigma_x$  is a constant of motion. For a massive particle,  $[\sigma_x, H_D] \neq 0$  and the evolution of the particle is described by

$$\hat{\mathbf{x}}(t) = \hat{\mathbf{x}}(0) + \hat{p}c^2 H_D^{-1} t + i\hat{\xi}(e^{2iH_D t/\hbar} - 1)$$

where  $\hat{\xi} = (1/2)\hbar c(\sigma_x - \hat{p}cH_D^{-1})H_D^{-1}$ . The first two terms represent evolution that is linear in time, as expected for a free particle, whereas the third, oscillating, term may induce Zitterbewegung.

For the simulation, we trapped a single  $^{40}\text{Ca}^+$  ion in a linear Paul trap<sup>22</sup> with axial trapping frequency  $\omega_{\text{ax}} = 2\pi \times 1.36$  MHz and radial trapping frequency  $\omega_{\text{rad}} = 2\pi \times 3$  MHz. Doppler cooling, optical pumping and resolved sideband cooling on the  $S_{1/2} \leftrightarrow D_{5/2}$  transition in a magnetic field of 4 G prepare the ion in the axial motional ground state and in the internal state  $|S_{1/2}, m_j = 1/2\rangle$  ( $m_j$ , magnetic quantum number). A narrow-linewidth laser at 729 nm couples the states  $\binom{0}{1} \equiv |S_{1/2}, m_j = 1/2\rangle$  and  $\binom{1}{0} \equiv |D_{5/2}, m_j = 3/2\rangle$ , which we identify as our spinor states. A bichromatic light field resonant with the upper and lower axial motional sidebands of the  $\binom{1}{0} \leftrightarrow \binom{0}{1}$  transition with appropriately set phases and frequency realizes the Hamiltonian<sup>7</sup>

$$H_D = 2\eta\Delta\tilde{\Omega}\sigma_x\hat{p} + \hbar\Omega\sigma_z \quad (1)$$

Here  $\Delta = \sqrt{\hbar/2\tilde{m}\omega_{\text{ax}}}$  is the size of the ground-state wavefunction, with  $\tilde{m}$  the ion's mass (not to be confused with the mass,  $m$ , of the

<sup>1</sup>Institut für Quantenoptik und Quanteninformation, Österreichische Akademie der Wissenschaften, Otto-Hittmair-Platz 1, A-6020 Innsbruck, Austria. <sup>2</sup>Institut für Experimentalphysik, Universität Innsbruck, Technikerstrasse 25, A-6020 Innsbruck, Austria. <sup>3</sup>Departamento de Química Física, Universidad del País Vasco - Euskal Herriko Unibertsitatea, Apartado 644, 48080 Bilbao, Spain. <sup>4</sup>IKERBASQUE, Basque Foundation for Science, Alameda Urquijo 36, 48011 Bilbao, Spain.

simulated particle);  $\eta = 0.06$  is the Lamb–Dicke parameter; and  $\hat{p} = i\hbar(a^\dagger - a)/2\Delta$  is the momentum operator, with  $a^\dagger$  and  $a$  the usual raising and lowering operators for the motional state along the axial direction. The first term in equation (1) describes a state-dependent motional excitation with coupling strength  $\eta\tilde{\Omega}$ , corresponding to a displacement of the ion’s wave packet in the harmonic trap. The parameter  $\tilde{\Omega}$  is controlled by setting the intensity of the bichromatic light field. The second term is equivalent to an optical Stark shift and occurs when the bichromatic light field is detuned from resonance by  $2\Omega$ . Equation (1) reduces to the 1 + 1 dimensional Dirac Hamiltonian if we make the identifications  $c \equiv 2\eta\tilde{\Omega}\Delta$  and  $mc^2 \equiv \hbar\Omega$ . The momentum and position of the Dirac particle are then mapped onto the corresponding quadratures of the trapped-ion harmonic oscillator.

To study relativistic effects such as Zitterbewegung, it is necessary to measure  $\langle \hat{x}(t) \rangle$ , the expectation value of the position operator of the harmonic oscillator. It has been noted theoretically that such expectation values could be measured using very short probe times, without reconstructing the full quantum state<sup>7,23,24</sup>. To measure  $\langle \hat{x} \rangle$  for a motional state  $\rho_m$ , we have to (1) prepare the ion’s internal state in an eigenstate of  $\sigma_y$ , (2) apply a unitary transformation,  $U(\tau)$ , that maps information about  $\rho_m$  onto the internal states and (3) record the changing excitation as a function of the probe time  $\tau$ , by measuring fluorescence<sup>22</sup>. In this protocol, the unitary operator  $U(\tau) = \exp(-i\eta\Omega_p\sigma_x\hat{x}\tau/\Delta)$ , with  $\hat{x} = (a^\dagger + a)\Delta$  and probe Rabi frequency  $\Omega_p$ , effectively transforms the observable  $\sigma_x$  into  $\sin k\hat{x}$ , with  $k = 2\eta\Omega_p\tau/\Delta$ , meaning that  $\langle \hat{x} \rangle$  can be determined by monitoring the rate of change of  $\langle \sin k\hat{x} \rangle$  for short probe times (Methods). Because the Dirac Hamiltonian generally entangles the motional and internal states of the ion, we first incoherently recombine the internal state population in  $\binom{0}{1}$  (Methods) before proceeding to step 1. Then we apply the Hamiltonian generating  $U$  with the probe Rabi frequency set to  $\Omega_p = 2\pi \times 13$  kHz for interaction times  $\tau$  of up to 14  $\mu\text{s}$ , in 1–2- $\mu\text{s}$  steps. The change of excitation was obtained by linear fits, each based on  $10^4$  to  $3 \times 10^4$  measurements.

We simulate the Dirac equation by applying  $H_D$  for varying amounts of time and for different particle masses. In the experiment,

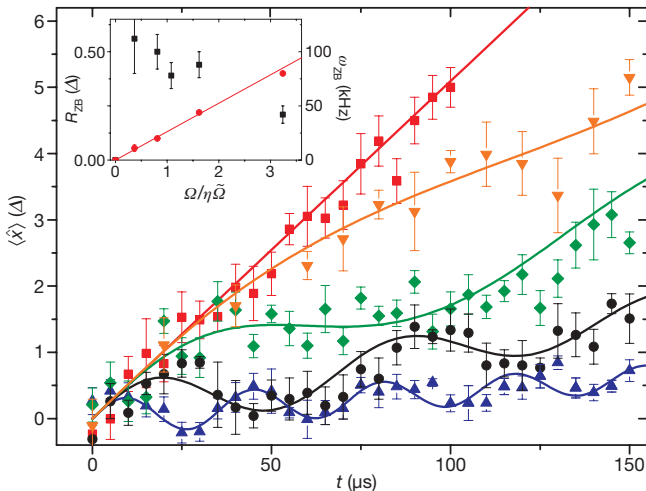


**Figure 1 | Expectation values,  $\langle \hat{x}(t) \rangle$ , for particles with different masses.** The linear curve (squares) represents a massless particle ( $\Omega = 0$ ) moving at the speed of light, which is given by  $c = 2\eta\tilde{\Omega}\Delta = 0.052\Delta \mu\text{s}^{-1}$  for all curves. From the top, the other curves represent particles of increasing masses. Their Compton wavelengths are given by  $\lambda_C \equiv 2\eta\tilde{\Omega}\Delta/\Omega = 5.4\Delta$  (down triangles),  $2.5\Delta$  (diamonds),  $1.2\Delta$  (circles) and  $0.6\Delta$  (up triangles), respectively. The solid curves represent numerical simulations. The figure shows Zitterbewegung for the crossover from the relativistic limit,  $2\eta\tilde{\Omega} \gg \Omega$ , to the non-relativistic limit,  $2\eta\tilde{\Omega} \ll \Omega$ . Inset, fitted Zitterbewegung amplitude,  $R_{ZB}$  (squares), and frequency,  $\omega_{ZB}$  (circles), versus the parameter  $\Omega/\eta\tilde{\Omega}$  (which is proportional to the mass). Error bars,  $1\sigma$ .

we set  $\tilde{\Omega} = 2\pi \times 68$  kHz, corresponding to a simulated speed of light of  $c = 0.052\Delta \mu\text{s}^{-1}$ . The measured expectation values,  $\langle \hat{x}(t) \rangle$ , are shown in Fig. 1 for a particle initially prepared in the spinor state  $\psi(x; t = 0) = (\sqrt{2\pi}2\Delta)^{-1/2} e^{-x^2/4\Delta^2} \binom{1}{1}$  by sideband cooling and application of a  $\pi/2$  pulse. Zitterbewegung appears for particles with non-zero mass, and is obtained by varying  $\Omega$  in the range  $0 < \Omega \leq 2\pi \times 13$  kHz by changing the detuning of the bichromatic lasers.

We investigate the particle dynamics in the crossover from relativistic to non-relativistic dynamics. The data in Fig. 1 well match numerical simulations based on equation (1), which are shown as solid lines. The error bars are obtained from a linear fit assuming quantum projection noise, which dominates noise caused by fluctuations of control parameters. In addition, the data were fitted with a heuristic model function of the form  $\langle \hat{x}(t) \rangle = at + R_{ZB}\sin\omega_{ZB}t$  to extract the effective amplitude,  $R_{ZB}$ , and frequency,  $\omega_{ZB}$ , of the Zitterbewegung shown in the inset. As the particle’s initial momentum is not dispersion free, the amplitude and frequency are only approximate concepts. From these data, it can be seen that the frequency,  $\omega_{ZB} \approx 2\Omega$ , grows linearly with increasing mass, whereas the amplitude decreases as the mass is increased. Because the mass of the particle increases but the momentum and the simulated speed of light remain constant, the data in Fig. 1 show the crossover from the far relativistic to non-relativistic limits. Hence, the data confirm that Zitterbewegung decreases in both limits, as theoretically expected. In the far-relativistic case, this is because  $\omega_{ZB}$  vanishes; in the non-relativistic case, it is because  $R_{ZB}$  vanishes.

The tools with which we simulate the Dirac equation can also be used to set the initial state of the simulated particle precisely. The particle in Fig. 2a was given an average initial momentum  $\langle \hat{p}(t = 0) \rangle = \hbar/\Delta$  by means of a displacement operation using the Hamiltonian  $H = \hbar\eta\Omega\sigma_x\hat{x}/\Delta$ . The initial state of this particle consists

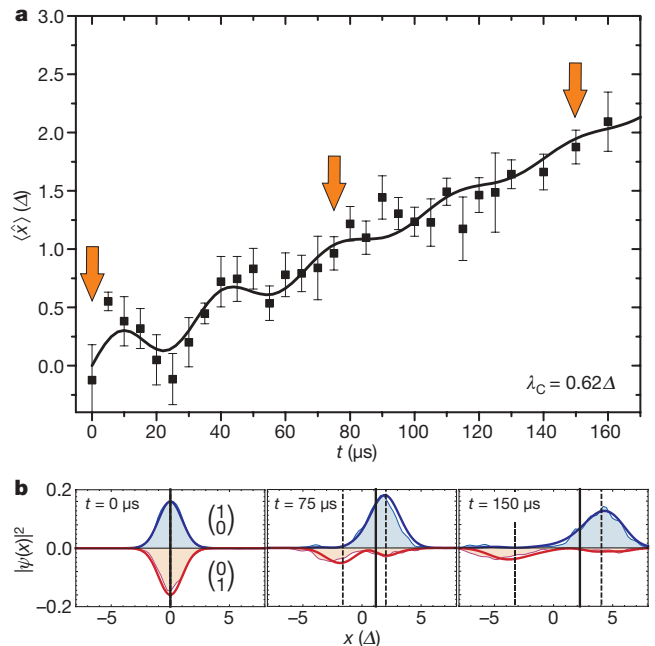


**Figure 2 | Zitterbewegung for a state with non-zero average momentum.** **a**, Initially, Zitterbewegung appears owing to interference of positive- and negative-energy parts of the state,  $\psi(x; t = 0) = e^{ix/\Delta} e^{-x^2/4\Delta^2} (\sqrt{2\pi}2\Delta)^{-1/2} \binom{1}{1}$ . As these parts separate, the oscillatory motion fades away. The solid curve represents a numerical simulation. Error bars,  $1\sigma$ . **b**, Measured (filled areas) and numerically calculated (solid lines) probability distributions,  $|\psi(x)|^2$ , at times  $t = 0, 75$  and  $150 \mu\text{s}$  (as indicated by the arrows in **a**). The probability distribution corresponding to the state  $\binom{0}{1}$  is inverted for clarity. The vertical solid line represents  $\langle \hat{x} \rangle$  as plotted in **a**. The two dashed lines indicate the respective expectation values for the positive- and negative-energy parts of the spinor.

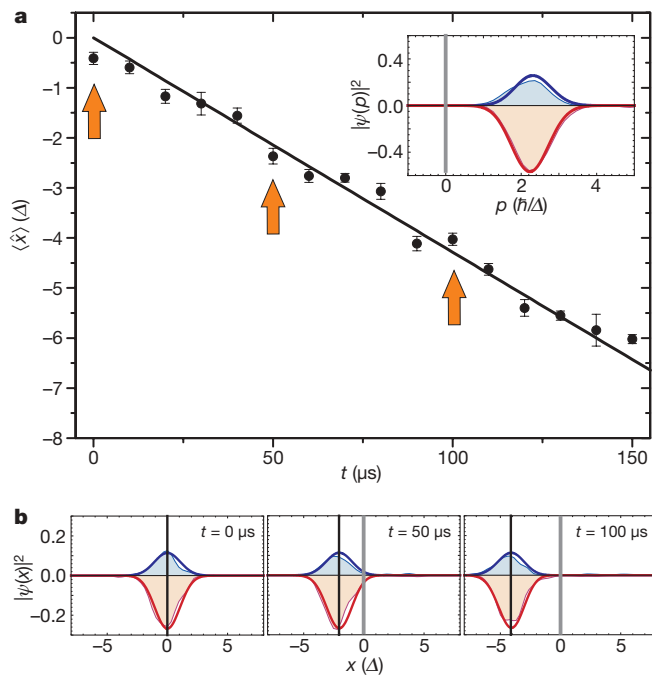


**Figure 3 | Time evolution of a negative-energy eigenstate with  $\lambda_c = 1.2\lambda$ .** Laser pulses create the spinor  $\psi(p; t = 0) = \sqrt{\Delta/\hbar} \begin{pmatrix} -0.48 \exp[-(p-2.26)^2 \Delta^2/\hbar^2] \\ 0.75 \exp[-(p-2.14)^2 \Delta^2/\hbar^2] \end{pmatrix}$ , which approximates a negative-energy spinor with average momentum  $\langle \hat{p} \rangle = 2.2\hbar/\Delta$ . The corresponding initial momentum distribution,  $|\tilde{\psi}(p)|^2$ , is shown in the inset. The filled curves represent data, whereas the solid lines represent a numerical calculation. The data in **a** show no Zitterbewegung. The solid curve represents a numerical simulation. Error bars,  $1\sigma$ . **b**, Measured probability distributions,  $|\psi(x)|^2$ , for three different evolution times (indicated by the arrows in **a**). There is no splitting of the wavefunction and the evolution and spreading is as intuitively expected for a free particle.

of a positive-energy component with positive velocity and a negative-energy component with negative velocity<sup>25</sup>. The positive-energy component moves to the right and is contributed to by both spinor states (Methods), whereas the negative-energy component moves to the left. Zitterbewegung is observed as long as these parts overlap, and dies out as they separate. Further information is obtained by a complete reconstruction of the probability distribution<sup>26</sup>  $|\psi(x)|^2$ , shown in Fig. 2b. It is also possible to initialize the spinor in a pure negative- or positive-energy state (Methods). In Fig. 3a, we show the time evolution,  $\langle \hat{x}(t) \rangle$ , of a negative-energy spinor with average momentum  $\langle \hat{p} \rangle = 2.2\hbar/\Delta$ . The corresponding reconstructed probability distributions are displayed in Fig. 3b, and it can be seen that there is neither Zitterbewegung nor splitting of the wavefunction, which occurs only if there are positive- and negative-energy contributions to the wavefunction.

We have implemented a proof-of-principle quantum optical simulation of a tunable relativistic quantum mechanical system. We have demonstrated that the simulated one-dimensional Dirac dynamics for a free particle shows Zitterbewegung and several of its counterintuitive quantum relativistic features. A natural route for the near future will be to move theoretically and experimentally towards the simulation of dynamics that are impossible (or difficult) to calculate in real systems, such as in quantum chemistry<sup>27</sup> or quantized Dirac fields in the context of quantum field theory<sup>1</sup>. Our experiment serves as a first step towards more complex quantum simulations. Furthermore, the mapping between quantum optical systems and relativistic quantum mechanics may be followed by further analogies between the Dirac dynamics and the Jaynes–Cummings model<sup>8,28,29</sup>, and in photonic<sup>9</sup> or sonic systems<sup>30</sup>.

## METHODS SUMMARY

Measurements in position space are carried out by mapping the observable of interest onto the ion's internal state. Applying a state-dependent displacement

operation,  $U = \exp(-ik\hat{x}\sigma_x/2)$ , to the quantum state  $\rho$ , followed by a measurement of  $\sigma_z$ , is equivalent to measuring the observable

$$A(k) = U^\dagger \sigma_z U = \cos(k\hat{x})\sigma_z + \sin(k\hat{x})\sigma_y$$

on the original state  $\rho$ , where  $k = 2\eta\Omega_p/\Delta$  is proportional to the interaction time,  $t$ . If the ion's internal initial state is the eigenstate of  $\sigma_z$  belonging to eigenvalue  $+1$ , then  $\langle A(k) \rangle = \langle \cos k\hat{x} \rangle$ . Similarly, for the eigenstate of  $\sigma_y$ , belonging to eigenvalue  $+1$ ,  $\langle A(k) \rangle = \langle \sin k\hat{x} \rangle$ . A Fourier transformation of these measurements yields the probability density  $|\psi(x)|^2$  in position space (or equivalently  $|\delta(\hat{x} - x)|^2$  if the state is not pure but mixed). Moreover, the coefficients of the Taylor expansion of the observable  $A(k)$  are proportional to the moments  $\hat{x}^n$ , and in particular  $d\langle A(k) \rangle/dk|_{k=0} \propto \langle \hat{x} \rangle$ . The reconstruction of the wave packets associated with the spinor components  $\begin{pmatrix} 1 \\ 0 \end{pmatrix}$  and  $\begin{pmatrix} 0 \\ 1 \end{pmatrix}$ , shown in Figs 2 and 3, is achieved by projecting either part of the wavefunction onto the  $D_{5/2}$  state using a fluorescence measurement followed by the measurement scheme based on post-selected data, described above.

To construct spinors with either purely positive- or negative-energy solutions, it is useful to express a general spinor as  $\psi = P^+ \psi + P^- \psi$ , that is, using the projection operations projecting onto the positive- and negative-energy contributions ( $E_\pm = \sqrt{c^2 p^2 + m^2 c^4}$ ). In momentum space, the projection operators are given by

$$P^\pm(p) = \frac{1}{2} \left( I_2 \pm \frac{cp\sigma_x + mc^2\sigma_z}{\sqrt{c^2 p^2 + m^2 c^4}} \right)$$

Here  $I_2$  is the  $2 \times 2$  identity matrix. The spinor state in Fig. 3 was 'reverse-engineered' by projecting out the negative-energy part of a wave packet with average momentum  $\langle \hat{p} \rangle = 2.2\hbar/\Delta$  and renormalizing the spinor. The relative contributions of the two spinor states, and the phase between them, can be set straightforwardly in the experiment. The momentum distributions can be approximated by Gaussians with appropriately set average momenta.

**Full Methods** and any associated references are available in the online version of the paper at [www.nature.com/nature](http://www.nature.com/nature).

**Received 31 August; accepted 11 November 2009.**

- Thaller, B. *The Dirac Equation* (Springer, 1992).
- Anderson, C. D. The positive electron. *Phys. Rev.* **43**, 491–494 (1933).
- Klein, O. Die Reflexion von Elektronen an einem Potentialsprung nach der relativistischen Dynamik von Dirac. *Z. Phys.* **53**, 157–165 (1929).
- Schrödinger, E. Über die kräftefreie Bewegung in der relativistischen Quantenmechanik. *Sitz. Preuss. Akad. Wiss. Phys.-Math. Kl.* **24**, 418–428 (1930).
- Garay, L. J., Anglin, J. R., Cirac, J. I. & Zoller, P. Sonic analog of gravitational black holes in Bose-Einstein condensates. *Phys. Rev. Lett.* **85**, 4643–4647 (2000).
- Schliemann, J., Loss, D. & Westervelt, R. M. Zitterbewegung of electronic wave packets in III–V zinc-blende semiconductor quantum wells. *Phys. Rev. Lett.* **94**, 206801 (2005).
- Lamata, L., León, J., Schätz, T. & Solano, E. Dirac equation and quantum relativistic effects in a single trapped ion. *Phys. Rev.* **98**, 253005 (2007).
- Bermudez, A., Martin-Delgado, M. A. & Solano, E. Exact mapping of the 2+1 Dirac oscillator onto the Jaynes-Cummings model: ion-trap experimental proposal. *Phys. Rev. A* **76**, 041801(R) (2007).
- Zhang, X. Observing Zitterbewegung for photons near the Dirac point of a two-dimensional photonic crystal. *Phys. Rev. Lett.* **100**, 113903 (2008).
- Vaishnav, J. Y. & Clark, C. W. Observing Zitterbewegung with ultracold atoms. *Phys. Rev. Lett.* **100**, 153002 (2008).
- Otterbach, J., Unanyan, R. G. & Fleischhauer, M. Confining stationary light: Dirac dynamics and Klein tunneling. *Phys. Rev. Lett.* **102**, 063602 (2009).
- Krekora, P., Su, Q. & Grobe, R. Relativistic electron localization and the lack of Zitterbewegung. *Phys. Rev. Lett.* **93**, 043004 (2004).
- Wang, Z.-Y. & Xiong, C.-D. Zitterbewegung by quantum field-theory considerations. *Phys. Rev. A* **77**, 045402 (2008).
- Feynman, R. Simulating physics with computers. *Int. J. Theor. Phys.* **21**, 467–488 (1982).
- Cserti, J. & Dávid, G. Unified description of Zitterbewegung for spintronic, graphene, and superconducting systems. *Phys. Rev. B* **74**, 172305 (2006).
- Katsnelson, M. I., Novoselov, K. S. & Geim, A. K. Chiral tunnelling and the Klein paradox in graphene. *Nature Phys.* **2**, 620–625 (2006).
- Neto, A. H. C., Guinea, F., Peres, N. M. R., Novoselov, K. S. & Geim, A. K. The electronic properties of graphene. *Rev. Mod. Phys.* **81**, 109–162 (2009).
- Leibfried, D. et al. Trapped-ion quantum simulator: experimental application to nonlinear interferometers. *Phys. Rev. Lett.* **89**, 247901 (2002).
- Porras, D. & Cirac, J. I. Effective quantum spin systems with trapped ions. *Phys. Rev. Lett.* **92**, 207901 (2004).
- Johanning, M., Varón, A. F. & Wunderlich, C. Quantum simulations with cold trapped ions. *J. Phys. B* **42**, 154009 (2009).
- Friedenauer, H., Schmitz, H., Glueckert, J., Porras, D. & Schaetz, T. Simulating a quantum magnet with trapped ions. *Nature Phys.* **4**, 757–761 (2008).
- Kirchmair, G. et al. Deterministic entanglement of ions in thermal states of motion. *New J. Phys.* **11**, 023002 (2009).

23. Lougovski, P., Walther, H. & Solano, E. Instantaneous measurement of field quadrature moments and entanglement. *Eur. Phys. J. D* **38**, 423–426 (2006).
24. Santos, M. F., Giedke, G. & Solano, E. Noise-free measurement of harmonic oscillators with instantaneous interactions. *Phys. Rev. Lett.* **98**, 020401 (2007).
25. Thaller, B. Visualizing the kinematics of relativistic wave packets. Preprint at (<http://arxiv.org/abs/quant-ph/0409079>) (2004).
26. Wallentowitz, S. & Vogel, W. Reconstruction of the quantum mechanical state of a trapped ion. *Phys. Rev. Lett.* **75**, 2932–2935 (1995).
27. Aspuru-Guzik, A., Dutoi, A. D., Love, P. J. & Head-Gordon, M. Simulated quantum computation of molecular energies. *Science* **309**, 1704–1707 (2005).
28. Rozmej, P. & Arvieu, R. The Dirac oscillator: a relativistic version of the Jaynes-Cummings model. *J. Phys. A* **32**, 5367–5382 (1999).
29. Bermudez, A., Martin-Delgado, M. A. & Solano, E. Dirac cat states in relativistic Landau levels. *Phys. Rev. Lett.* **99**, 123602 (2007).
30. Zhang, X. & Liu, Z. Extremal transmission and beating effect of acoustic waves in two-dimensional sonic crystals. *Phys. Rev. Lett.* **101**, 264303 (2008).

**Acknowledgements** We gratefully acknowledge support from the Austrian Science Fund, the European Commission (Marie-Curie programme) and the Institut für Quanteninformation GmbH. E.S. acknowledges support of Universidad del País Vasco - Euskal Herriko Unibertsitatea grant GIU07/40 and European Union project EuroSQIP. This material is based upon work supported in part by Intelligence Advanced Research Projects Activity. We thank H. Häffner and M. Baranov for comments on the manuscript.

**Author Contributions** G.K., F.Z. and R.G. performed the experiment and analysed the data; E.S. provided the theoretical analysis; C.F.R. and R.G. designed the experiment and carried out numerical simulations; R.B., G.K., F.Z., R.G. and C.F.R. contributed to the experimental set-up; and all authors co-wrote the paper.

**Author Information** Reprints and permissions information is available at [www.nature.com/reprints](http://www.nature.com/reprints). The authors declare no competing financial interests. Correspondence and requests for materials should be addressed to C.F.R. ([christian.roos@uibk.ac.at](mailto:christian.roos@uibk.ac.at)).

## METHODS

**Measurement of  $\langle \hat{x} \rangle$  and  $|\psi(x)|^2$ .** In ion-trap experiments, the only observable that can directly be measured by fluorescence detection is  $\sigma_z$ . Additional laser pulses can be used to map other observables onto  $\sigma_z$ . In the experiment, we apply a state-dependent displacement operation,  $U = \exp(-ik\hat{x}\sigma_x/2)$ , to the quantum state  $\rho$ , and then measure  $\sigma_z$ , which is equivalent to measuring the observable

$$A(k) = U^\dagger \sigma_z U = \cos(k\hat{x})\sigma_z + \sin(k\hat{x})\sigma_y$$

on the initial state  $\rho$ , because  $\text{Tr}((U^\dagger \rho U)\sigma_z) = \text{Tr}(\rho(U\sigma_z U^\dagger))$ . Here  $k = 2\eta\Omega_p t/\Delta$  is proportional to the interaction time,  $t$ . We have  $\langle A(k) \rangle = \langle \cos k\hat{x} \rangle$  if the ion's internal initial state is prepared in the eigenstate of  $\sigma_z$  belonging to eigenvalue  $+1$ ; for an ion prepared in the eigenstate of  $\sigma_y$  belonging to eigenvalue  $+1$ , we obtain  $\langle A(k) \rangle = \langle \sin k\hat{x} \rangle$ . A Fourier transformation of these measurements yields the probability density  $|\psi(x)|^2$  in position space.

For the position operator, we have  $d\langle A(k) \rangle/dk|_{t=0} \propto \langle \hat{x}\sigma_y \rangle$ . Measuring  $\langle \hat{x} \rangle$  thus requires the preparation of an eigenstate of  $\sigma_y$ , which cannot be done directly when the motional state is entangled with the internal state. To solve this problem, we first incoherently recombine the internal state in  $\begin{pmatrix} 0 \\ 1 \end{pmatrix}$ . This is done by first shelving the population initially in  $\begin{pmatrix} 0 \\ 1 \end{pmatrix}$  to  $|D_{5/2}, m_j = 5/2\rangle$  using a rapid adiabatic passage transfer. A second such transfer shifts the population in  $\begin{pmatrix} 1 \\ 0 \end{pmatrix}$  to  $\begin{pmatrix} 0 \\ 1 \end{pmatrix}$ . A 100- $\mu\text{s}$  laser pulse at 854 nm transfers the population in  $|D_{5/2}, m_j = 5/2\rangle$  to  $|P_{3/2}, m_j = 3/2\rangle$ , from which it spontaneously decays to  $\begin{pmatrix} 0 \\ 1 \end{pmatrix}$ . The transfer efficiency is  $>99\%$ , limited by the small branching ratio to the  $D_{3/2}$  state. In the transfer steps, a probability exists that the motional state of the ion is changed. This probability is however very small, owing to the small Lamb–Dicke parameter, but could be eliminated completely by a separate measurement of the motional states of the spinor states  $\begin{pmatrix} 0 \\ 1 \end{pmatrix}$  and  $\begin{pmatrix} 1 \\ 0 \end{pmatrix}$ , at the expense of a longer data acquisition time.

To distinguish between populations in the states  $\begin{pmatrix} 1 \\ 0 \end{pmatrix}$  and  $\begin{pmatrix} 0 \\ 1 \end{pmatrix}$ , when reconstructing  $|\psi(x)|^2$  (as shown in Figs 2 and 3), we applied a short (200- $\mu\text{s}$ ) fluorescence detection to measure the internal state. We used only cases in which  $\begin{pmatrix} 1 \\ 0 \end{pmatrix}$  was measured (leaving the motional state unchanged as no photons were scattered) for the subsequent analysis. To reconstruct  $|\psi(x)|^2$  belonging to  $\begin{pmatrix} 0 \\ 1 \end{pmatrix}$ , a  $\pi$  pulse before the short detection was used to interchange the internal state populations. **Constructing a pure negative-energy spinor.** A general spinor is built up out of positive- and negative-energy components (energies  $E_\pm = \pm\sqrt{c^2 p^2 + m^2 c^4}$ ) such that  $\psi = P^+ \psi + P^- \psi$ . In momentum space, the projection operators are given by

$$P^\pm(p) = \frac{1}{2} \left( I_2 \pm \frac{cp\sigma_x + mc^2\sigma_z}{\sqrt{c^2 p^2 + m^2 c^4}} \right) \quad (2)$$

Here  $I_2$  is the  $2 \times 2$  identity matrix. In general, the projection operators do not project onto the spinor basis states. The exception is when  $p = 0$ , because in this case the projector in equation (2) becomes diagonal in the spinor basis. The spinor state in Fig. 3 was ‘reverse-engineered’ by projecting out the negative-energy part of a wave packet with average momentum  $\langle \hat{p} \rangle = 2.2\hbar/\Delta$  and renormalizing the spinor.

The complete sequence for approximating the negative-energy state is conveniently described in the basis of the eigenstates  $|\pm\rangle_y = (1/\sqrt{2})\begin{pmatrix} 1 \\ \pm i \end{pmatrix}$  of  $\sigma_y$ . After ground-state cooling, we prepare the state  $|+\rangle_y$ . Then we displace this state to one with average momentum  $\langle \hat{p} \rangle = 2.2\hbar/\Delta$  by using the displacement Hamiltonian  $H = \hbar\eta\tilde{\Omega}\sigma_y\hat{x}/\Delta$ . Next, a far-detuned laser pulse rotates the internal state to  $0.84|+\rangle_y + i0.53|-\rangle_y$ . The displacement Hamiltonian  $H = -\hbar\eta\tilde{\Omega}\sigma_y\hat{x}/\Delta$  shifts these parts in opposite directions to create the required asymmetry between the average momenta of the components. A final  $\pi/2$  pulse creates the state shown in Fig. 3. This state has  $>99\%$  overlap with the desired negative-energy state.